Advanced Composite Materials
Publication details, including instructions for authors and subscription information:
http://www.tandfonline.com/loi/tacm20

Flexural properties of a hybrid polymer matrix composite containing carbon and silicon carbide fibres

I. J. Davies [a] & H. Hamada [b]

[a] Advanced Fibro-Science, Kyoto Institute of Technology, Matsugasaki, Sakyo-ku, Kyoto 606-8585, Japan

[b] Advanced Fibro-Science, Kyoto Institute of Technology, Matsugasaki, Sakyo-ku, Kyoto 606-8585, Japan

Version of record first published: 02 Apr 2012.

To cite this article: I. J. Davies & H. Hamada (2001): Flexural properties of a hybrid polymer matrix composite containing carbon and silicon carbide fibres , Advanced Composite Materials, 10:1, 77-96

To link to this article: http://dx.doi.org/10.1163/15685510152546376

Adv. Composite Mater., Vol. 10, No. 1, pp. 77–96 (2001)

Flexural properties of a hybrid polymer matrix composite containing carbon and silicon carbide fibres

I. J. DAVIES * and H. HAMADA

Advanced Fibro-Science, Kyoto Institute of Technology, Matsugasaki, Sakyo-ku, Kyoto 606-8585, Japan

Received 23 August 2000; accepted 28 September 2000

Abstract—The flexural properties of hybrid unidirectional fibre reinforced polymer (FRP) composites containing a mixture of carbon (C) and silicon carbide (SiC) fibres were evaluated at span-to-depth (S/d) ratios of 16, 32, and 64. The flexural strength generally increased with increasing S/d ratio with a maximum value of 2316 MPa being achieved for the specimen with nominally equal volume fractions of C and SiC fibre. However, even replacing 12.5 vol% of the C fibres by SiC fibres increased the flexural strength by 22%. The mechanical property most strongly influenced by the incorporation of SiC fibres was the work of fracture with a maximum value of 206.5 kJ m^{-2} (compared to 78.8 kJ m^{-2} for the specimen containing only C fibres). First estimate values for the SiC fibre compressive strength, elastic modulus, and strain to failure were 3.46 GPa, 157 GPa, and 0.018, respectively.

Keywords: Hybrid polymer matrix composite; flexural properties; silicon carbide fibres; carbon fibres.

1. INTRODUCTION

The superior tensile properties of carbon fibre reinforced polymer (CFRP) composites, combined with their relatively low density, have led to numerous applications, such as those of sports equipment, aerospace structures, and reinforcement of civil engineering structures [1]. However, it is also known that the crystalline microstructure of carbon fibres [2, 3] results in a compressive strength that is significantly less compared to their tensile strength [4–7]. Figure 1 illustrates the compressive and tensile strength for typical carbon fibres [8] with the compressive strength in all cases being approximately 30–50% that of the respective tensile strength. The relatively poor compressive strength of carbon fibres translates itself into a reduced compressive performance of CFRP composites [9, 10] and thus may hinder the acceptance of these materials in certain applications. For example, it has been reported

*To whom correspondence should be addressed. E-mail: davies@ipc.kit.ac.jp

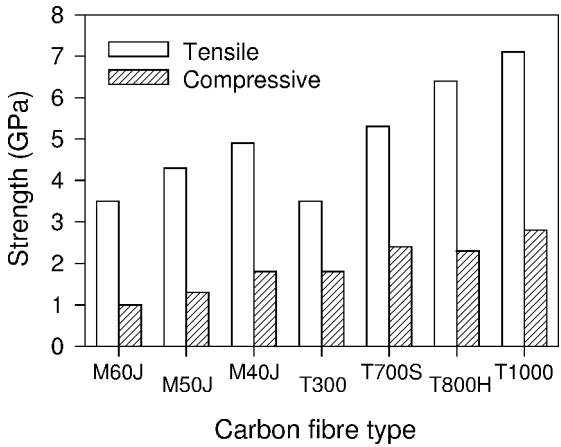

Figure 1. Relationship between tensile and compressive strength for different carbon fibres [8].

that the tensile strength of unidirectional T700S/epoxy CFRP composite is 2.3 GPa whereas the compressive strength is only 1.1 GPa [9].

One approach to improving the compressive properties of CFRP composites may be the partial substitution of carbon fibres by other fibres possessing superior compressive strength. Although there is a lack of quantitative data, it has been suggested that the compressive strength of fibres based on the silicon carbide (SiC) system may exceed that of carbon fibres due to the amorphous or nano-crystalline structure of the former [11, 12]. For example, the compressive strength of unidirectional SiC/epoxy FRP composite is reported to be in excess of 2 GPa [13]. Preliminary work [13–15] to investigate the mechanical properties of fibre reinforced polymer (FRP) composites containing a mixture of C and SiC fibres showed an increase in compressive strength when a proportion of the C fibres was replaced by SiC fibres. However, the C fibres utilised in those investigations (HTA-6000) possessed relatively poor tensile strength (3.6 GPa) and thus would also be expected to exhibit low compressive strength. Therefore, a more valid comparison would be for the case of FRP composites containing high compressive strength C fibres.

The present authors have undertaken a preliminary investigation in order to determine the mechanical properties of high compressive strength CFRP composites in which a proportion of the C fibres were replaced by SiC fibres. The present work focuses on the flexural properties of such materials whilst a companion paper will consider properties measured in compression [16].

2. EXPERIMENTAL

The present investigation was conducted for unidirectional FRP composites containing a mixture of C fibres (Type T700S, Toray, Tokyo, Japan), SiC-based fibres (Tyranno Si-Ti-C-O fibre, Grade S, Ube Industries Ltd., Ube City, Japan), and epoxy matrix (Epikote 828, Yuka Shell Epoxy Co. Ltd., Tokyo, Japan). The composites

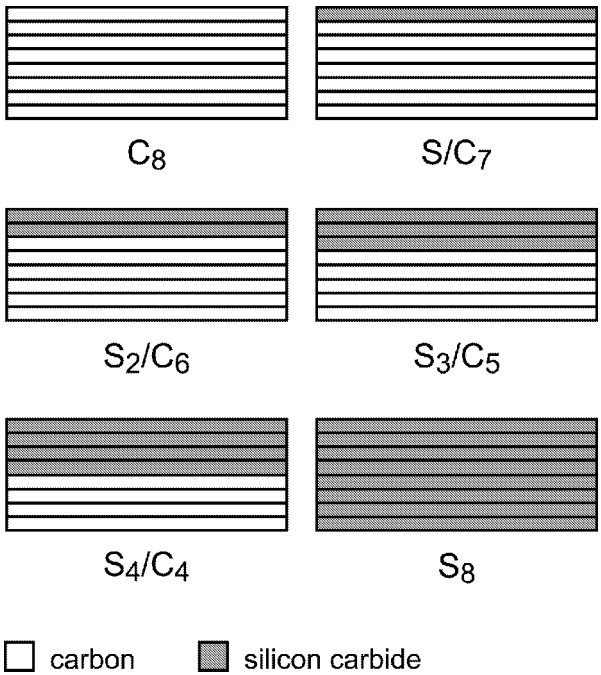

Figure 2. Schematic representation of the layer configuration in the composite specimens.

were produced by first winding either SiC or C fibres through an acetone solution of resin and hardener onto a cylindrical mandrel and then heating for 20 min at 120°C in order to produce a prepreg sheet. The prepreg sheets were then cut to approximately 80 × 150 mm and stacked into an eight layer sequence with a total of six different layer configurations being tested in the present work (Fig. 2). The resulting unidirectional reinforced plates were heated in vacuum and held for 30 min at 120°C under a pressure of ∼2.5 MPa in order to produce a composite plate with ∼2 mm thickness. The fibre volume fraction, V_f, was calculated from areal image analysis of scanning electron micrographs and found to be approximately 0.67 for all specimens. In contrast to this, the specimen density increased from 1.60 g cm^{-3} (C_8) to 2.09 g cm^{-3} (S_8) and this was accounted for using manufacturer supplied data for the density of the SiC, C, and epoxy components (2.35 g cm^{-3}, 1.8 g cm^{-3}, and 1.16 g cm^{-3}, respectively).

Specimens for flexural testing were cut into beams of width 6.5 mm and tested in the three point bend configuration using spans of 32 mm, 64 mm, and 128 mm, i.e. nominal span-to-depth, S/d, ratios of 16, 32, and 64, respectively, using a standard mechanical testing machine (Model 4206, Instron Ltd., Japan) and 10 mm diameter rollers. All of the specimens containing SiC fibre were positioned with the SiC fibres nearest to the compressive surface. Crosshead speeds of 0.5 mm min^{-1}, 1 mm min^{-1}, and 2 mm min^{-1} were used for S/d values of 16, 32, and 64, respectively. The maximum compressive strain, ε_C^*, and maximum tensile strain,

ε_T^*, at the specimen surface were measured by placing strain gauges (5 mm gauge length) adjacent to the middle roller and also on the opposite tensile surface directly below the middle roller.

The flexural strength, σ, was calculated using the maximum load whilst the elastic modulus, E, was determined at a strain, ε, of 2.5×10^{-3}. In addition, the specific flexural strength and elastic modulus (i.e. mechanical property divided by density) were calculated and presented as σ' and E', respectively. All averaged data presented in this work possessed a typical error less than 5% and usually on the order of 2–3%. Following failure, the side edges of specimens (i.e. showing a cross-section between the tensile and compressive faces) parallel to the specimen main axis were examined using low magnification optical microscopy after being embedded in mounting resin and polished to a 5 μm surface finish.

3. RESULTS AND DISCUSSION

3.1. Span to depth ratio of 16

The effect of SiC fibre content and span to depth ratio on σ and σ' has been presented in Fig. 3. Considering first the data for the case of $S/d = 16$, the C_8 specimen (containing no SiC fibre) exhibited a flexural strength (Fig. 3a) of 1361 MPa which increased to 1527 MPa for the case of the S/C_7 specimen

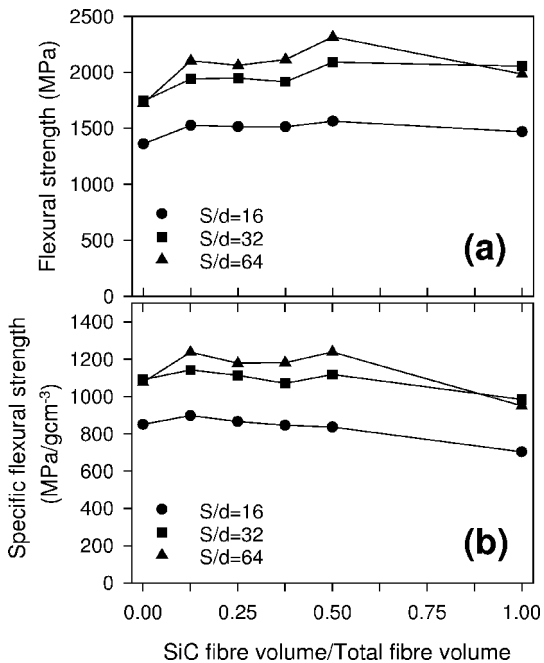

Figure 3. Effect of span-to-depth ratio (S/d) and SiC fibre volume fraction on: (a) flexural strength, and (b) specific flexural strength.

containing 0.125 V_f SiC fibre (as a fraction of the total fibre volume), then decreased slightly for the S_2/C_6 and S_3/C_5 specimens and reached a peak of 1564 MPa for the S_4/C_4 specimen with 0.5 V_f SiC fibre. However, the S_8 specimen containing only SiC fibre showed a slight decrease to 1470 MPa. From these data, it would appear that the partial substitution of C fibre by SiC fibre may produce a significant increase (up to 15%) in flexural strength for $S/d = 16$, whereas total substitution provides only an 8% increase. In many applications, such as those of aerospace and space, specific properties are a key parameter when comparing the performance of different materials. Thus, although the S_4/C_4 specimen possessed the maximum σ, Fig. 3b illustrates that σ' was maximum for the S/C_7 specimen (899 MPa/g cm^{-3}) and 6% larger compared to that of the C_8 specimen. The difference in trends for σ and σ' may be directly attributed to the larger density of the SiC fibre (2.35 g cm^{-3}) compared to the C fibre (1.8 g cm^{-3}). Indeed, the value of σ' for the S_8 specimen was 17% less than that of the C_8 specimen. The above data thus indicates that, for $S/d = 16$, σ is maximum for the S_4/C_4 specimen whilst σ' is maximum for the S/C_7 specimen.

Considering the effect of SiC fibre content on E and E' (Fig. 4) for $S/d = 16$, no significant trend in E was noted with increasing SiC content; all specimens being within the range 83–95 GPa. In contrast to this, the C_8 specimen possessed the highest E' (55.9 GPa/g cm^{-3}) which decreased with increasing SiC content to a

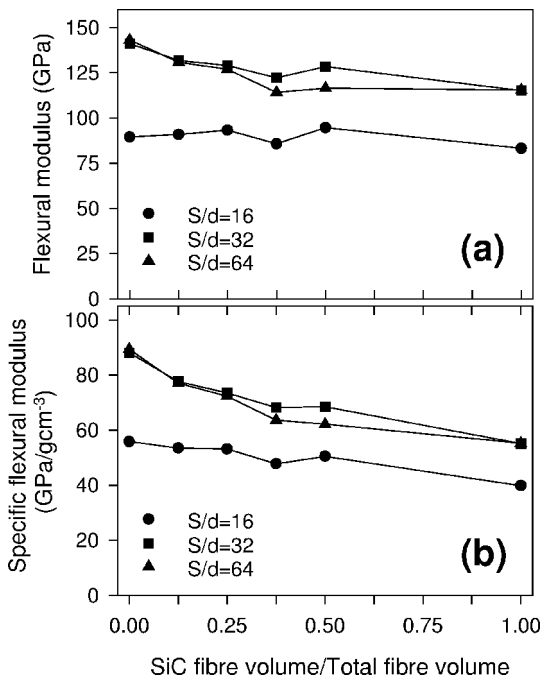

Figure 4. Effect of span-to-depth ratio (S/d) and SiC fibre volume fraction on: (a) flexural modulus, and (b) specific flexural modulus.

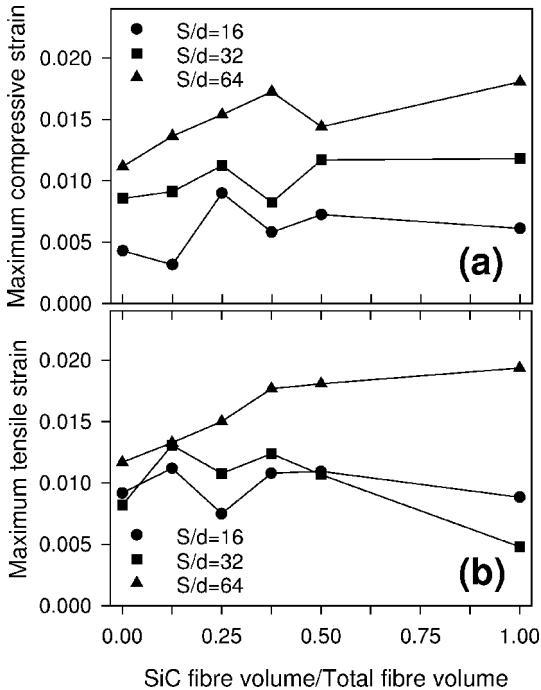

Figure 5. Effect of span-to-depth ratio (S/d) and SiC fibre volume fraction on: (a) maximum compressive strain, and (b) maximum tensile strain.

minimum of 39.9 GPa/g cm^{-3} for the S_8 specimen; this trend again being directly attributed to the higher SiC fibre density.

Data for ε_C^* and ε_T^* (Fig. 5) taken from representative specimens appeared difficult to interpret for $S/d = 16$ due to the lack of any significant trend. It can be noted that ε_T^* (Fig. 5b) was generally larger than ε_C^* (Fig. 5a) and this can be seen more closely in the load *vs.* strain curves shown in Fig. 6a. However, whereas the strain gauge at the tensile face could be placed at the expected point of ε_T^* (i.e. at the position opposite the middle roller), this was not possible for the strain gauge at the compressive face (i.e. at the position of the middle roller). Thus, for this reason, ε_C^* in Fig. 5a would be less than the actual ε_C^* experienced within the specimen. This phenomenon may explain to some extent the difference in magnitude between ε_C^* and ε_T^* for the case of $S/d = 16$ in Fig. 5.

Regarding the type of failure experienced by the specimens for $S/d = 16$, specimens containing up to 0.375 V_f SiC fibre (i.e. C_8, S/C_7, S_2/C_6, and S_3/C_5) failed beneath the middle roller at the compressive face (i.e. at the point of maximum compressive stress and strain) with an example of this being presented in Fig. 7. Magnification of the failure region (Fig. 7b) showed clear evidence of out-of-plane fibre microbuckling or kinking [17] with it being observed that the specimen side edges possessed ridges just beneath the middle roller due to the fibres kinking out-of-plane. Fibre microbuckling and kinking are widely

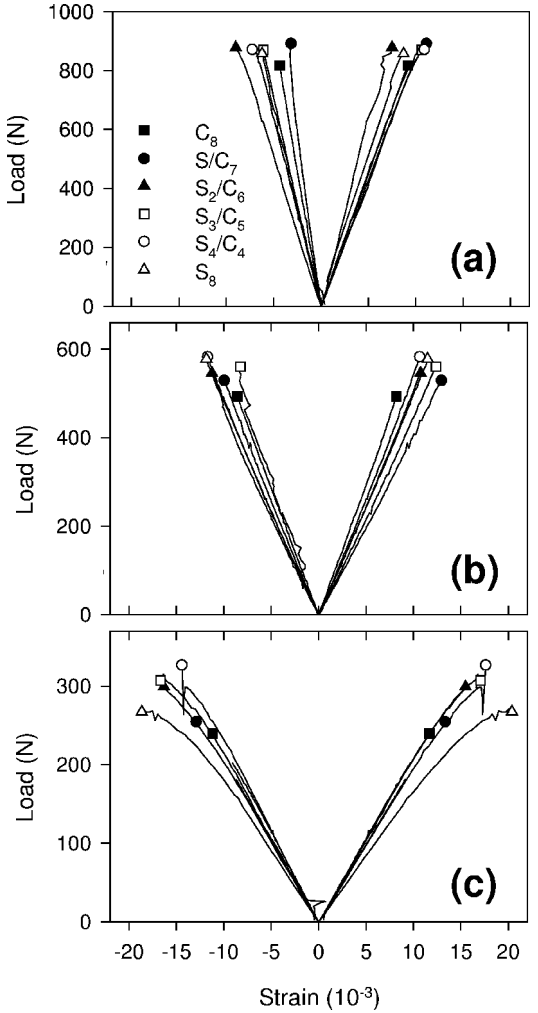

Figure 6. Relationship between load and strain at the compressive and tensile faces for different span-to-depth ratios: (a) 16, (b) 32, and (c) 64. Note that the legends in (a) also apply to (b) and (c).

known to occur in unidirectional CFRP composites and has been the subject of significant research [17–27]; it is thus not surprising that these phenomena occur within the region of compressive stress in flexural specimens. The initiation of fibre microbuckling has been linked to misalignment of fibres in the direction of compressive loading [27]. Regarding three-point bend flexural testing, the load introduced into the specimen by the middle roller will also result in misalignment of the fibres (due to curvature of the specimen) with respect to the direction of maximum compressive force and this is believed to be the reason behind the microbuckling failure. In contrast to this, the specimens with 0.5 and 1.0 V_f SiC fibre (i.e. S_4/C_4 and S_8, respectively) exhibited shear failure at the specimen mid-point, resulting in specimen delamination as shown in Fig. 8. Shear and delamination

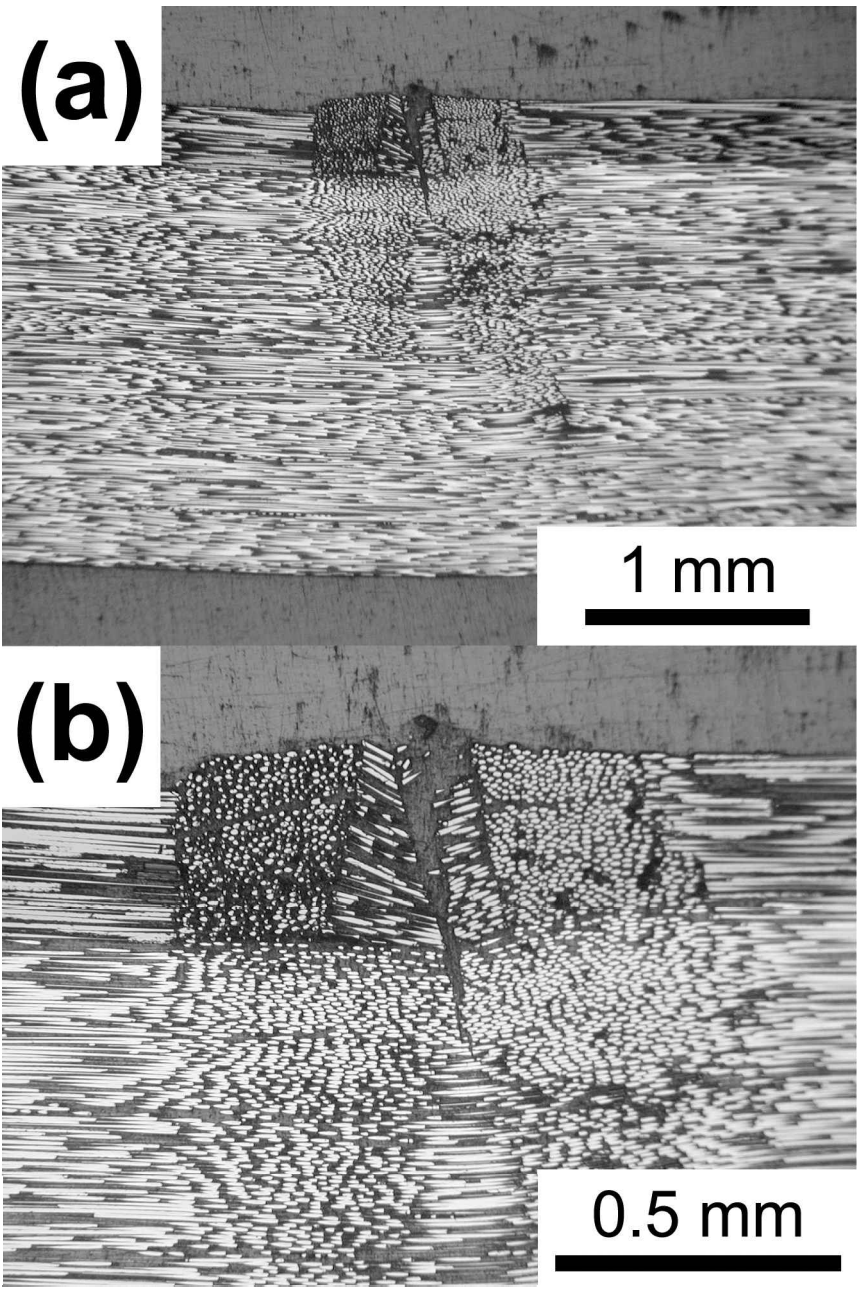

Figure 7. Optical micrographs illustrating failure of the S/C_7 specimen at $S/d = 16$: (a) general view, and (b) detailed view.

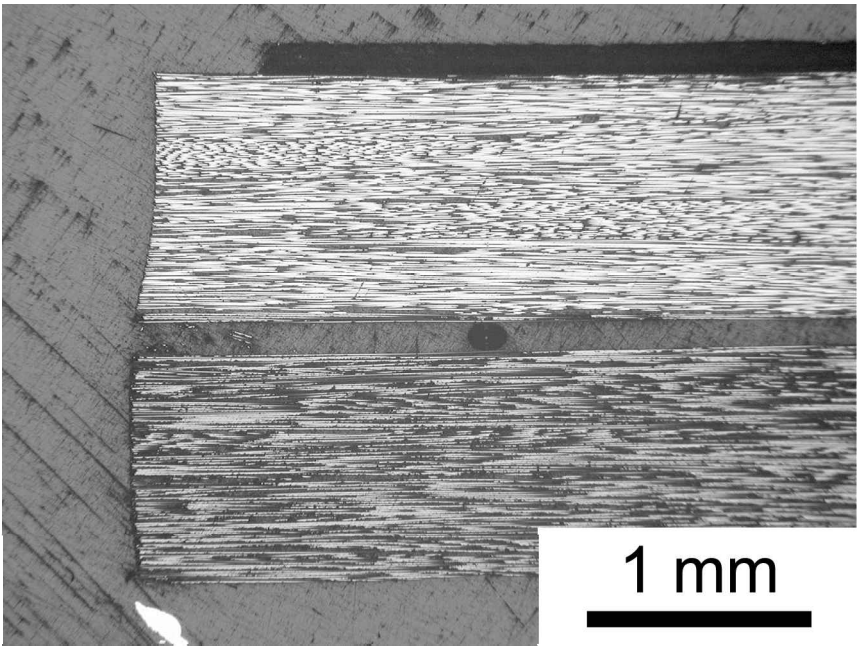

Figure 8. Optical micrograph illustrating failure of the S_4/C_4 specimen at $S/d = 16$.

failure of unidirectional FRP specimens subject to flexural loading is known to be a problem, particularly for small S/d ratios. The explanation for this is that the flexural strength for the three point bend configuration can be given by:

$$\sigma = \frac{3 \cdot F \cdot S}{2 \cdot b \cdot d^2}, \tag{1}$$

where F is the maximum load (units: N) and b is the specimen width (units: m). Compared to this, the maximum shear stress, τ, at the neutral axis can be given by:

$$\tau = \frac{3 \cdot F}{4 \cdot b \cdot d}. \tag{2}$$

The ratio between σ and τ can then be given by:

$$\frac{\sigma}{\tau} = \frac{2 \cdot S}{d}. \tag{3}$$

Thus, at small values of S/d, a specimen of low shear strength is expected to fail by shear at the neutral axis. Alternatively, if we assume that τ is similar for the specimens under investigation (a reasonable hypothesis [14]), then shear failure will be most likely to occur in those specimens with highest compressive or tensile strength. The fact that the specimens with high SiC V_f exhibited shear failure may allow us to deduce that these specimens should possess the highest flexural strengths

(when pure compressive or tensile strength is the limiting factor) provided that S/d is sufficiently large.

3.2. Span to depth ratio of 32

Although the basic trend was similar, compared to the case of $S/d = 16$, it can be seen from Fig. 3a that σ was significantly (up to 34%) higher for $S/d = 32$. The flexural strength was 1745 MPa for the C_8 specimen and increased by 11% to 1942 MPa for the S/C_7 specimen to reach a maximum value of 2090 MPa for the S_4/C_4 specimen. This general increase in σ with increasing SiC V_f was broadly similar to that noted by previous researchers [13–15]. On the other hand, Fig. 3b shows that σ' was 1089 MPa/g cm^{-3} for the C_8 specimen and increased to a maximum of 1144 MPa/g cm^{-3} for the S/C_7 specimen.

Whereas the trend in σ was essentially similar for S/d values of 16 and 32, the data for E (Fig. 4a) showed a more pronounced decrease with increasing SiC V_f for $S/d = 32$ than had been the case for $S/d = 16$. It is noted that E was maximum for the C_8 specimen (141.0 GPa) and then decreased to a minimum of 115.1 GPa for the S_8 specimen whilst E' was a maximum of 88.1 GPa/g cm^{-3} for the C_8 specimen and decreased to 55.1 GPa/g cm^{-3} for the S_8 specimen. Using E for the S_8 specimen (115.1 GPa) together with data for the compressive modulus of the epoxy matrix ($\approx$30 GPa [29]), a first approximation for the SiC fibre compressive modulus was determined to be 157 GPa — somewhat below the SiC fibre tensile modulus (175 GPa [13]). The significant overall increase in E for $S/d = 32$, compared to $S/d = 16$, was attributed to the reduced effect of shear deformation when calculating E for the $S/d = 32$ case [28]. Namely, the derivation of the flexural modulus equation assumes there to be negligible specimen deformation due to shear stresses; this assumption is most likely not true for low S/d ratios with the result that E is underestimated [28]. Such a phenomenon has previously been reported [28] in E-glass/polyester composites with E increasing with increasing S/d ratio and $S/d \geqslant 40$ being recommended for the accurate determination of E.

The increase in σ for the $S/d = 32$ specimens was mirrored in the higher values of ε_C^* (Fig. 5a) (although the values of ε_T^* overall appeared similar for both the $S/d = 16$ and $S/d = 32$ cases) indicating that the compressive face of the specimens sustained a higher stress prior to failure. The increase in ε_C^*, and hence σ, was attributed to two different factors: (i) for the C_8, S/C_7, S_2/C_6, and S_3/C_5 specimens, the larger S/d ratio meant that specimen curvature (i.e. fibre misalignment parallel to the applied compressive force) was reduced upon loading to any given compressive stress, meaning that a higher compressive stress was required to induce microbuckling, and (ii) for the S_4/C_4 and S_8 specimens, the larger S/d ratio meant that shear failure was less likely to occur compared to other means of failure (from equation (3) and thus the flexural strength should increase. Similar to the case of $S/d = 16$, the load *vs.* strain curves were essentially linear to failure for all specimens tested at $S/d = 32$ (Fig. 6b).

Optical microscopy indicated that all specimens tested at $S/d = 32$ failed due to out-of-plane fibre microbuckling or kinking in the region of highest compressive stress beneath the middle roller. Most of the specimens exhibited a wedge-shaped failure mode (Fig. 9b), also referred to as a pair of conjugate kinks [21], comprising regions of kinked fibres surrounding a core of unbuckled fibres; this type of feature has been observed in carbon fibre-epoxy composites that failed in compression [19]. Another failure mode observed (Fig. 10) appeared to be characterized by a partially formed pair of conjugate kinks. The V-shaped feature to the right of centre in Fig. 10a appeared at first sight to comprise only of kinked fibres but on closer examination (Fig. 10b) was noted to contain a small wedge of intact fibres at the specimen surface. On the other hand, the feature to the left of centre in Fig. 10a comprised of a narrow kink band running approximately two thirds of the specimen depth. Such a phenomenon (i.e. a pair of conjugate kinks together with a single kink) has also been occasionally noted in CFRP composites [19]. In most specimens (such as Figs 9 and 10) there appeared to be little, if anything, in the way of shear failure and delamination. In fact, the only specimen that exhibited any significant delamination was the S_8 specimen (Fig. 11) which showed evidence of delamination cracks in addition to a wedge structure. Note that the pair of conjugate kinks in this case was not fully formed, as the left kink did not extend fully between the wedge root and specimen surface (Fig. 11b).

3.3. Span-to-depth ratio of 64

Increasing the S/d ratio from 32 to 64 resulted in a further slight increase in σ for most specimens on the order of 5–10% (Fig. 3a), indicating an S/d ratio of 32 to be insufficient when testing this composite system. The value of σ increased from 1722 MPa for the C_8 specimen to 2104 MPa for the S/C_7 specimen; a 22% increase from the substitution of 0.125 V_f of C fibres by SiC fibres. The strength leveled off for the S_2/C_6 and S_3/C_5 specimens but then reached a maximum of 2316 MPa for the S_4/C_4 specimen before decreasing to 1985 MPa for the S_8 specimen. The maximum increase in strength through partial substitution of C fibres by SiC was thus approximately 35%. The flexural strength of the C8 specimen was considerably greater compared to the compressive strength of T700S/epoxy composites (1058 MPa [9]) whereas that of the S_8 specimen was similar to the compressive strength of SiC/epoxy composites (2010 MPa [13]). Considering the maximum σ obtained in this study (2316 MPa) and the known V_f ($\approx$0.67), a first estimate for the compressive strength of the SiC fibres might be 3.46 GPa and similar to their tensile strength (3.3 GPa [13]).

One interesting point of note is that σ for the C_8 and S_8 specimens was similar for S/d ratios of 32 and 64, suggesting FRP composites containing only C or SiC fibre to not be as strong in compression when compared to the hybrid configurations; the reasoning behind this being that equation (3) provides that σ should increase with increasing S/d ratio and then level off when the 'true' flexural strength value is reached. The fact that the C_8 and S_8 specimens leveled off whereas the other

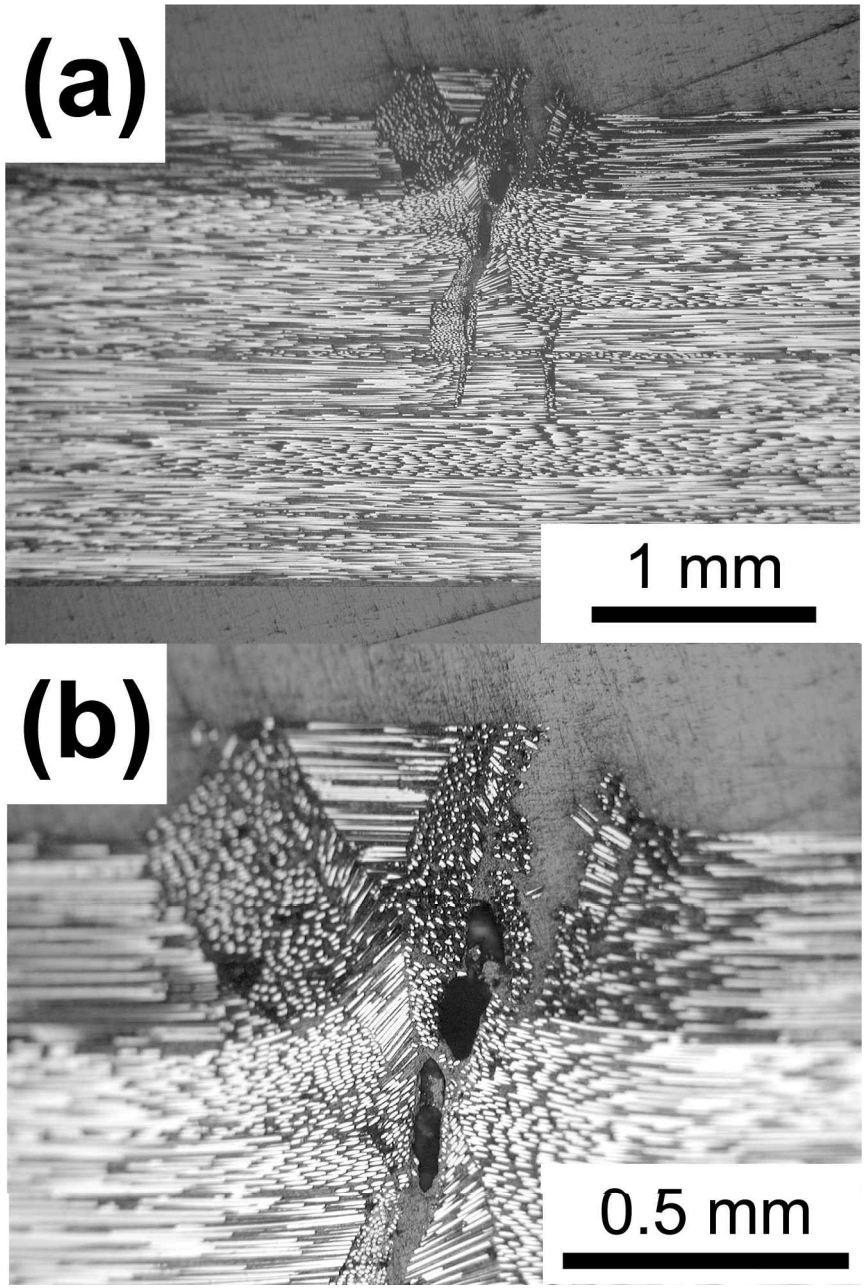

Figure 9. Optical micrographs illustrating failure of the S/C_7 specimen at $S/d = 32$: (a) general view, and (b) detailed view.

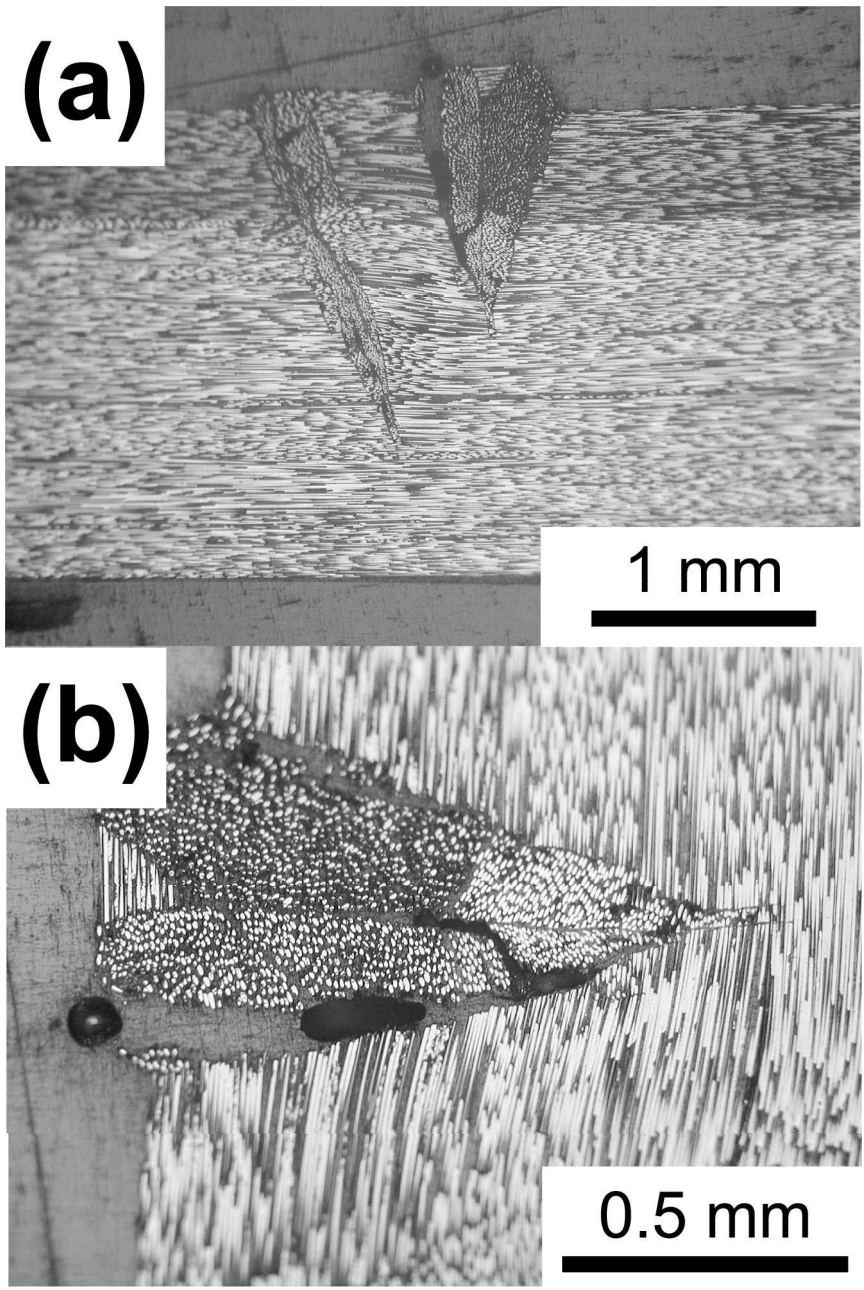

Figure 10. Optical micrographs illustrating failure of the S_2/C_6 specimen at $S/d = 32$: (a) general view, and (b) detailed view.

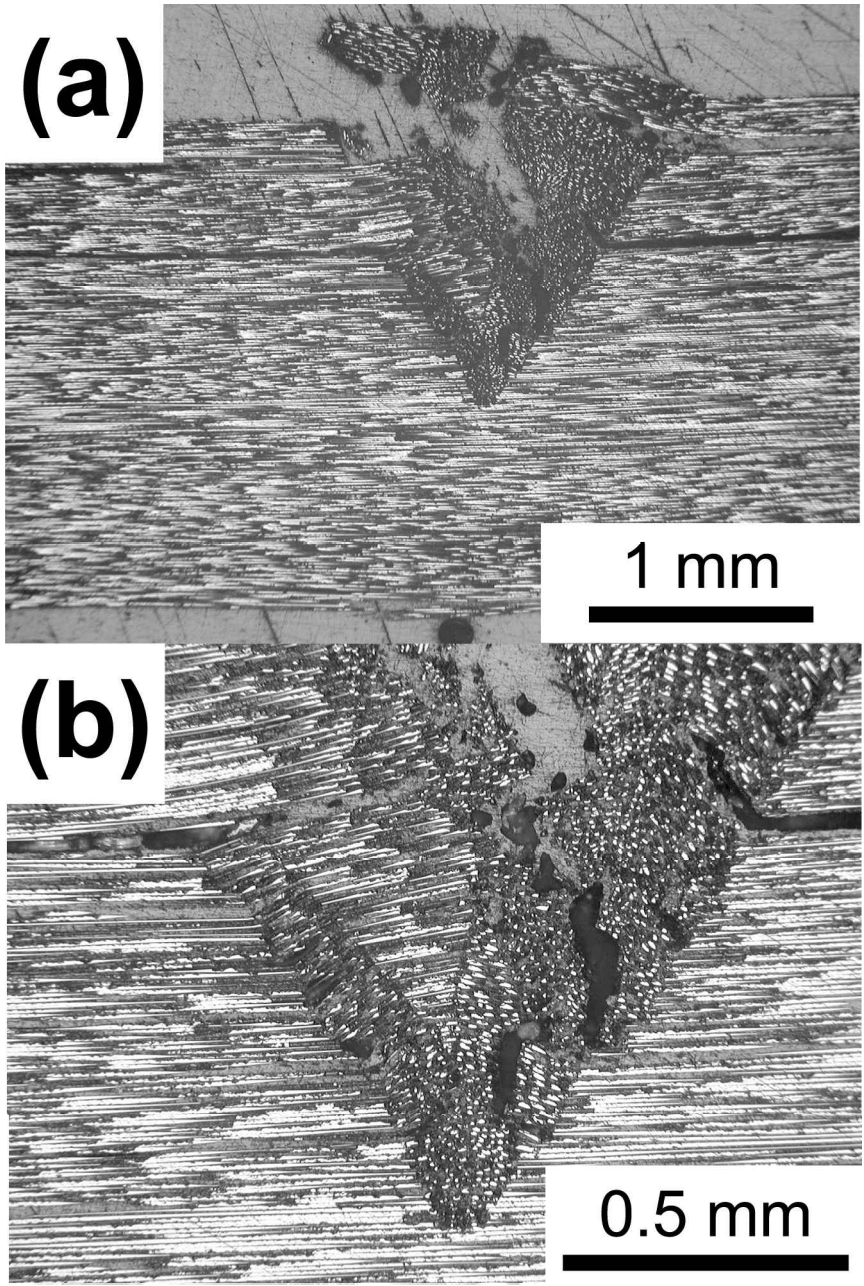

Figure 11. Optical micrographs illustrating failure of the S_8 specimen at $S/d = 32$: (a) general view, and (b) detailed view.

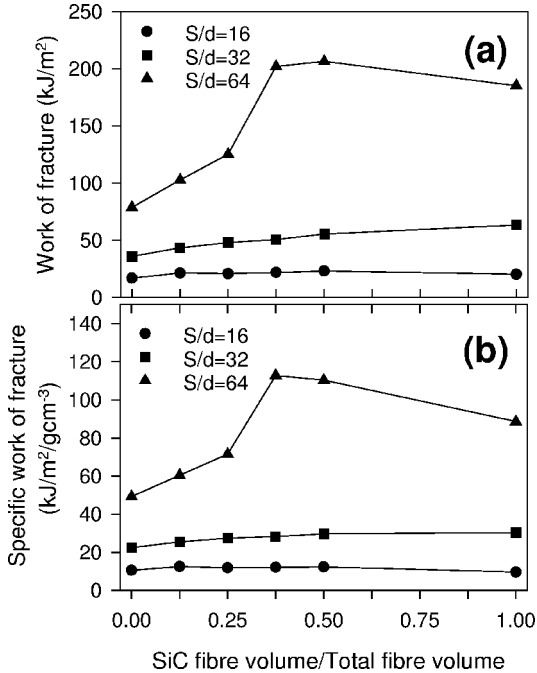

Figure 12. Effect of span-to-depth ratio (S/d) and SiC fibre volume fraction on: (a) work of fracture, and (b) specific work of fracture.

specimens did not suggests that the C_8 and S_8 specimens have lower intrinsic σ values compared to the other specimens. Put another way, if the shear strength is assumed to be similar for all specimens, then higher strength composites will require a higher S/d ratio before their σ values level off. There is thus the chance that even higher values of σ than those shown in Fig. 3a may be achieved at S/d ratios greater than 64.

Comparing the σ' data in Fig. 3b, an increase of 15% was noted between the C_8 specimen (1076.3 MPa/g cm^{-3}) and the S/C_7 specimen (1237.6 MPa/g cm^{-3}). Further increase in the SiC fibre V_f resulted in a slight decrease for the S_2/C_6 and S_3/C_5 specimens before reaching a maximum of 1238.5 MPa/g cm^{-3} for the S_4/C_4 specimen. Thus, maximum σ was achieved for the S_4/C_4 specimen whereas maximum σ' was found to be almost identical for the S/C_7 and S_4/C_4 specimens.

The ε_C^* and ε_T^* data (Fig. 5) exhibited similar trends with significant increases being noted for increasing SiC V_f. Maximum values of ε_C^* (0.0181) and ε_T^* (0.0194) were both achieved for the S_8 specimen, which is somewhat surprising considering that the S_8 specimen did not possess the largest σ; it may be interesting to test the S_8 specimen with an S/d ratio larger than 64 in order to determine whether further increases in σ may be obtained. The maximum value of ε_T^* (0.0194) is similar to that of ε_T^* for the SiC fibres [13] whereas we may consider that ε_C^* for the SiC fibres should, as a first approximation, be equal to or greater than the maximum ε_C^* determined in this work, i.e. 0.0181.

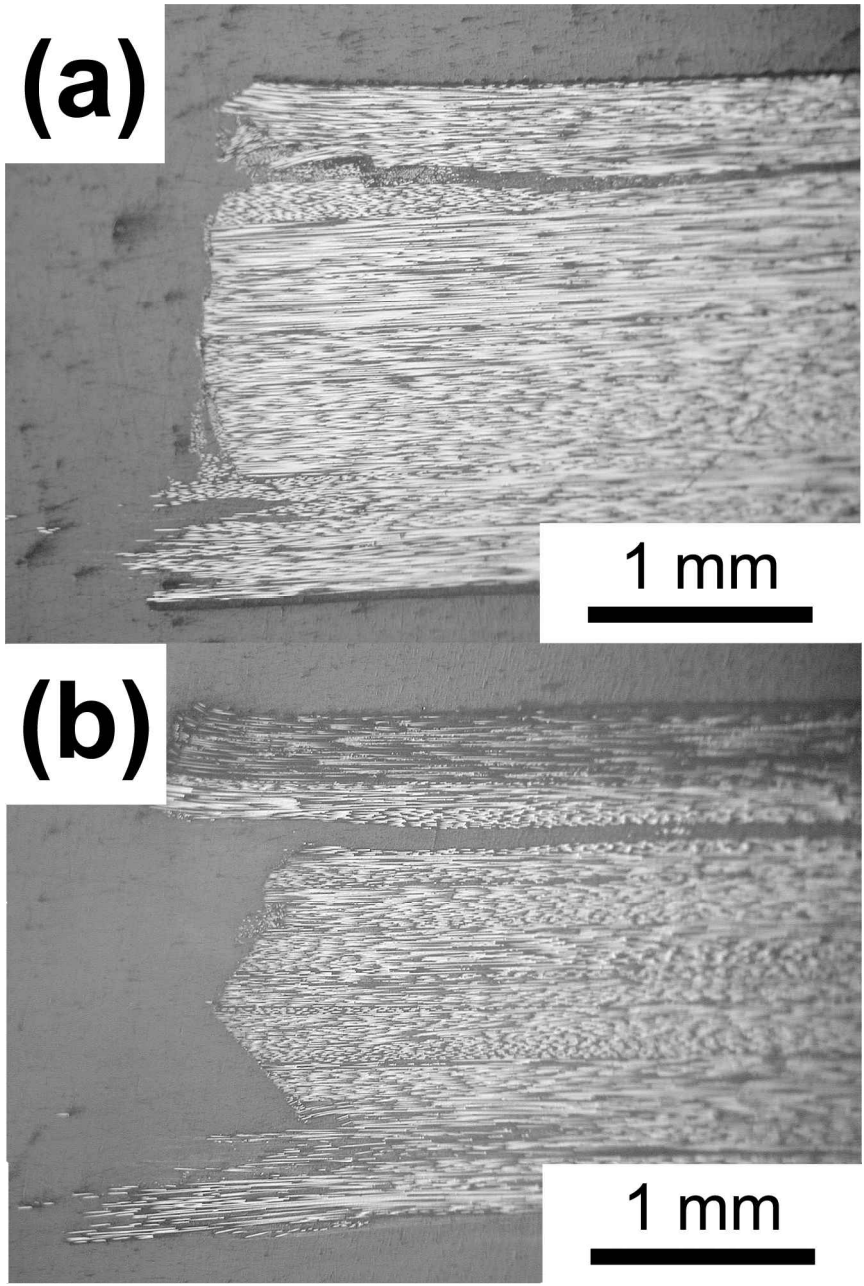

Figure 13. Optical micrographs illustrating failure at $S/d = 64$: (a) C_8 specimen, and (b) S/C_7 specimen.

Although σ was similar for the case of S/d ratios of 32 and 64, the load *vs.* strain data was considerably different (Fig. 6c) with a strong non-linear appearance to most of the specimens at $S/d = 64$; Fig. 6c also showed there to be large differences in load *vs.* strain behaviour for the different specimens. In order to investigate this further, the area under the force *vs.* displacement curve divided by the nominal surface area created during fracture (i.e. work of fracture, γ) was calculated with results being presented in Fig. 12. It can be seen for the $S/d = 64$ case that γ was minimum for the C_8 specimen (78.8 kJ m^{-2}) and increased by a factor of 2.4 for the S_8 specimen (185.3 kJ m^{-2}) with a maximum increase of 2.6 for the S_4/C_4 specimen (206.5 kJ m^{-2}). Even taking into account the higher density of the SiC fibre, the specific work of fracture, γ', was still a factor of 1.8 higher for the S_8 specimen (88.6 kJ m^{-2}/g cm^{-3}) compared to the C_8 specimen (49.3 kJ m^{-2}/g cm^{-3}) whilst γ' was maximum for the S_3/C_5 specimen (112.8 kJ m^{-2}/g cm^{-3}). The large increase in γ due to the partial substitution of C fibres by SiC fibres indicates that further investigation is warranted for the utilisation of such hybrid FRP composites in energy absorption applications such as crash impact structures.

The failure mode was also considerably different for the $S/d = 64$ specimens in that several of the specimens (C_8, S_2/C_8, and S_3/C_5) broke into two pieces exhibiting an almost flat fracture surface (Fig. 13a) in addition to a single delamination within the region under compression and the suggestion of fibre pullout close to the tensile surface. On the other hand, the S/C_7 specimen exhibited an unusual failure mode (Fig. 13b) with the appearance of shear failure in the middle half of the specimen together with delamination close to the compressive surface and fibre pullout close to the tensile surface. Perhaps surprisingly, there was no evidence of fibre microbuckling or kinks at the shear failure edges. The S_4/C_4 specimen fracture surface (Fig. 14) was dominated by multiple delamination in the compressive region together with a diagonal fracture surface in the middle portion and a small amount of fibre pullout at the tensile surface. The only specimen that did not break into two pieces was the S_8 specimen, which exhibited multiple delaminations throughout its width. The presence of multiple delaminations in the S_4/C_4 and S_8 specimens suggests that the shear strength may still be relatively too low in these specimens and that larger values of S/d may lead to further increases in σ.

4. CONCLUSIONS

Unidirectional FRP composites containing a mixture of C and SiC fibres were tested under flexural loading with the following conclusions:

(i) Flexural strength, maximum strain, and work of fracture generally increased with increasing S/d whilst flexural modulus increased significantly from $S/d = 16$ to $S/d = 32$.

(ii) The hybrid composite flexural strength was generally higher than either the pure CFRP or SiC fibre composites. The maximum flexural strength achieved

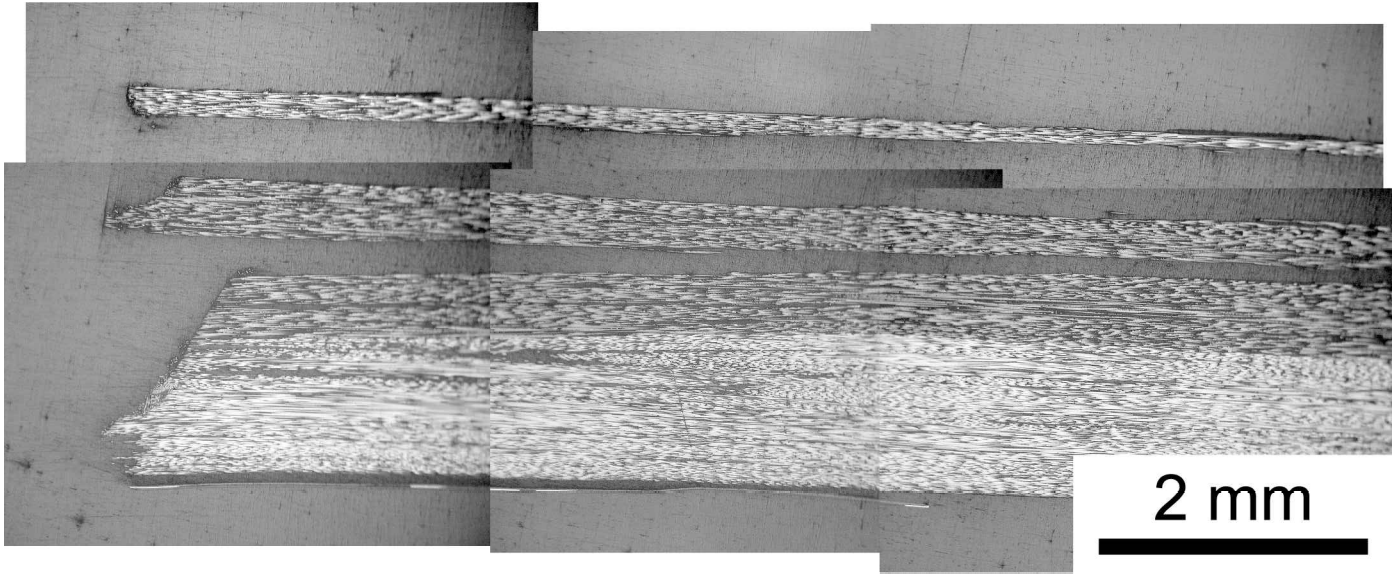

Figure 14. Optical micrograph illustrating failure of the S_4/C_4 specimen at $S/d = 64$.

was 2316 MPa whilst the maximum specific flexural strength was 1239 MPa/g cm^{-3}.

(iii) The work of fracture was a factor of 2.6 larger for the S_4/C_4 specimen compared to the S_8 specimen and suggests that these hybrid FRP composites may have a role as energy absorption materials.

(iv) The compressive stress, modulus, and strain to failure of the SiC fibre were estimated to be 3.46 GPa, 157 GPa, and 0.018, respectively.

(v) Most of the specimens exhibited out-of-plane pairs of conjugate kinks although specimens with larger SiC fibre V_f were more inclined to show evidence of shear failure.

(vi) It was suspected that further increasing S/d above 64 may result in higher flexural strength values for several of the specimens.

Acknowledgements

The authors wish to express their sincere thanks to Dr. M. Shibuya of Ube Industries, Ltd., for provision of the Tyranno Si-Ti-C-O fibres, Mr. T. Ohki for specimen preparation, and the original reviewer for invaluable comments.

REFERENCES

1. A. Takeo, Development of carbon fiber industry past and future, in: *Proc. 9th United States–Japan Conference on Composite Materials*, H. Fukuda, T. Ishikawa and Y. Kogo (Eds), pp. 15–22. Japan Society for Composite Materials, Tokyo (2000).
2. M. G. Dobb, H. Guo, D. J. Johnson and C. R. Park, Structure-compressional property relation in carbon fiber, *Carbon* **33**, 1553–1559 (1995).
3. M. Nakatani, M. Shioya and J. Yamashita, Axial compressive fracture of carbon fibers, *Carbon* **37**, 601–608 (1999).
4. H. M. Hawthorne and E. Teghtsoonian, Axial compression fracture in carbon fibres, *J. Mater. Sci.* **10**, 41–51 (1975).
5. M. Furuyama, M. Higuchi, K. Kubomura, H. Sunago, H. Jiang and S. Kumar, Compressive properties of single-filament carbon fibres, *J. Mater. Sci.* **28**, 1611–1616 (1993).
6. F. Watanabe, S. Ishida, Y. Korai, I. Mochida, I. Kato, Y. Sakai and M. Kamatsu, Pitch-based carbon fiber of high compressive strength prepared from synthetic isotropic pitch containing mesophase spheres, *Carbon* **37**, 961–967 (1999).
7. M. Shioya and M. Nakatani, Compressive strengths of single carbon fibres and composite strands, *Compas. Sci. Technol.* **60**, 219–229 (2000).
8. N. Oya and D. J. Johnson, Longitudinal compressive behaviour and microstructure of PAN-based carbon fibres, *Carbon* (in press).
9. N. Oya and H. Hamada, Effects of reinforcing fibre properties on various mechanical behaviour of unidirectional carbon/epoxy laminates, *Sci. Eng. Comp. Mater.* **5**, 105–129 (1996).
10. N. Oya and H. Hamada, Mechanical properties and failure mechanisms of carbon fibre reinforced thermoplastic laminates, *Composites Part A* **28A**, 823–832 (1997).
11. R. Bodet, X. Bourrat, J. Lamon and R. Naslain, Tensile creep behaviour of a silicon carbide-based fibre with a low oxygen content, *J. Mater. Sci.* **30**, 661–677 (1995).

12. Y. Xu, A. Zangvil, J. Lipowitz, J. A. Rabe and G. A. Zank, Microstructure and microchemistry of polymer-derived crystalline SiC fibers, *J. Amer. Ceram. Soc.* **76**, 3034–3040 (1993).
13. Manufacturers data, Technical report 6-001009, Ube Industries, Ltd., Ube City, Japan.
14. O. Hiroyuki and H. Tsujihata, *Goseijyushi Kogyo (Industrial Synthetic Resins)* **4**, 151–153 (1991).
15. O. Hiroyuki and H. Tsujihata, *Goseijyushi Kogyo (Industrial Synthetic Resins)* **3**, 106–107 (1992).
16. I. J. Davies and H. Hamada, Compressive properties of a hybrid polymer matrix composite containing carbon and silicon carbide fibres (in preparation).
17. A. G. Evans and W. F. Adler, Kinking as a mode of structural degradation in carbon fiber composites, *Acta Metall.* **26**, 725–738 (1978).
18. K. Kendall, Interfacial cracking of a composite: Part 3, compression, *J. Mater. Sci.* **11**, 1267–1269 (1976).
19. C. W. Weaver and J. G. Williams, Deformation of a carbon–epoxy composite under hydrostatic pressure, *J. Mater. Sci.* **10**, 1323–1333 (1975).
20. P. S. Steif, A model for kinking in fiber composites — I. Fiber breakage via micro-buckling, *Int. J. Solids Struct.* **26**, 549–561 (1990).
21. P. S. Steif, A model for kinking in fiber composites — II. Kink band formation, *Int. J. Solids Struct.* **26**, 563–569 (1990).
22. M. P. F. Sutcliffe and N. A. Fleck, Microbuckle propagation in carbon fibre–epoxy composites, *Acta Metall. Mater.* **42**, 2219–2231 (1994).
23. P. M. Moran, X. H. Liu and C. F. Shih, Kink band formation and band broadening in fiber composites under compressive loading, *Acta Metall. Mater.* **43**, 2943–2958 (1995).
24. S. Sivashanker, N. A. Fleck and M. P. F. Sutcliffe, Microbuckle propagation in a unidirectional carbon fibre–epoxy matrix composite, *Acta Mater.* **44**, 2581–2590 (1996).
25. T. J. Vogler and S. Kyriakides, Initiation and axial propagation of kink bands in fiber composites, *Acta Mater.* **45**, 2443–2454 (1997).
26. M. P. F. Sutcliffe and N. A. Fleck, Microbuckle propagation in fibre composites, *Acta Mater.* **45**, 921–932 (1997).
27. P. Berbinau, C. Soutis, P. Goutas and P. T. Curtis, Effect of off-axis ply orientation on 0°-fibre microbuckling, *Composites: Part A* **30**, 1197–1207 (1999).
28. G. Tolf and P. Clarin, Comparison between flexural and tensile modulus of fibre composites, *Fibre Sci. Technol.* **21**, 319–326 (1984).
29. K. Selby and L. E. Miller, Fracture toughness and mechanical behaviour of an epoxy resin, *J. Mater. Sci.* **12**, 12–24 (1975).